

## An Euler Calculation for a Hovering Coaxial Rotor Flow Field with New Boundary Condition

Référence : AE04

Kwanjung Yee<sup>\*</sup>, Dong-Ho Lee<sup>†</sup>

Department of Aerospace Engineering, Seoul National University  
Seoul 151-742, Korea

### ABSTRACT

In the present work, the flow field for a coaxial rotor in hover was computed numerically by employing the compressible Euler equations on embedded and moving patched grids. A sliding boundary was introduced to allow the relative motion between the upper and lower rotor, where the flow field information was interpolated by using moving patched algorithm. The vorticity confinement method (VCM) is applied so as to minimize the numerical diffusion but the results indicate that the inappropriate imposition of empirical parameter may cause a numerical instability. The computation was performed for a hovering coaxial rotor with rectangular planform of aspect ratio six. The results are compared with Nagashima's experiment and illustrate the feasibility of the present numerical approach in solving a coaxial rotor flow field.

### Nomenclature

$\alpha_{\text{TPP}}$	= tip path plane angle
$C_T$	= thrust coefficient
$c$	= chord length
$D$	= rotor diameter
$H$	= vertical distance between the rotors
$\theta_c$	= collective pitch angle
$\sigma$	= solidity
$\psi$	= angle between the blades
$\Omega$	= angular velocity
$\mu$	= advance ratio

### subscript

l	= lower
u	= upper
tip	= blade tip

---

\* Postdoctoral Research Associate

† Professor

### 1. Introduction

In recent years, the coaxial rotor configuration has renewed interests for its applicability to Unmanned Aerial Vehicles(UAV) and ship launched vehicles<sup>1</sup>. In the coaxial rotor, fuselage torque is compensated by utilizing two superimposed rotors, rotating in opposite direction. The coaxial design has the advantage of having its over-all dimensions defined only by the rotor diameter and of saving of power over the single rotor-tail rotor design<sup>2</sup>. On the other hand the rotor hubs and controls become more complex and rotor weights tend to increase.

Russia has been the leading countries in the development of the coaxial rotor design but the very few works are published in the west<sup>1</sup>. Nagashima conducted a program to study the aerodynamics of the coaxial rotor configuration in

hover and forward flight during the late 1970's and early 1980's<sup>1,3</sup>. Extensive experimental tests were performed to understand the wake structure and its relationship to rotor performance as a function of collective, rotor spacing and thrust level. But the previous researches concentrated mainly on the experiment and theoretical analyses and were very helpful in understanding the overall performance and physics. However, since they deal with the time-averaged aerodynamic coefficients, the unsteady aerodynamic characteristics of the flow field were not fully identified. The numerical studies on this problem are relatively rare<sup>4</sup> until now maybe due to the following difficulties: (1) Although the computer capacity has greatly improved these days, a large amount of computation time is still required for three dimensional unsteady flow field analysis. Moreover, in order to calculate the upper and lower rotors simultaneously, a larger computation domain is necessary; (2) In the same context mentioned above, a special consideration is needed in order to suppress the numerical diffusion due to the coarse grid density; (3) A proper wake modeling is not available for coaxial rotor configuration. Landgrebe<sup>5</sup> type prescribed wake model can not be applied to this rotor configuration because the shape and behavior of the coaxial rotor wake are quite different from those of a single rotor.;(4) A very complex grid strategy is required to handle moving grid configuration and it is almost impossible to construct the whole flow field in a single block.

The main objective of this work is to introduce a new boundary condition for a coaxial rotor analysis and to check the applicability of vorticity confinement technique. The accuracy

and feasibility of the present work is validated

## 2. Governing Equation

While the hovering can be regarded as a steady problem for a single rotor calculation, the coaxial rotor flow field is intrinsically unsteady even for a hovering. Therefore, the governing Euler equations should be described in the inertial coordinate system to handle the general grid motion<sup>6,7</sup>.

$$\frac{1}{J} \frac{\partial Q}{\partial \tau} + \frac{\partial \hat{E}}{\partial \xi} + \frac{\partial \hat{F}}{\partial \eta} + \frac{\partial \hat{G}}{\partial \zeta} = 0$$

$$Q = \begin{bmatrix} \rho \\ \rho u \\ \rho v \\ \rho w \\ e \end{bmatrix} \quad \hat{E} = \frac{1}{J} \begin{bmatrix} \rho U \\ \rho u U + \xi_x p \\ \rho v U + \xi_y p \\ \rho w U + \xi_z p \\ (e+p)U - p\xi_t \end{bmatrix}$$

$$\hat{F} = \frac{1}{J} \begin{bmatrix} \rho V \\ \rho u V + \eta_x p \\ \rho v V + \eta_y p \\ \rho w V + \eta_z p \\ (e+p)V - p\eta_t \end{bmatrix} \quad \hat{G} = \frac{1}{J} \begin{bmatrix} \rho W \\ \rho u W + \zeta_x p \\ \rho v W + \zeta_y p \\ \rho w W + \zeta_z p \\ (e+p)W - p\zeta_t \end{bmatrix}$$

From the state equation for an ideal gas, the energy is obtained from the following relation,

$$p = (\gamma - 1) \left\{ e - \frac{1}{2} \rho (u^2 + v^2 + w^2) \right\}$$

The convective terms are discretized using Roe's flux difference splitting<sup>8</sup>.

$$\hat{E}_{i+1/2} = \frac{1}{2} \{ \hat{E}_{i,j} + \hat{E}_{i+1,j} - \hat{A} | (Q_{i+1,j} - Q_{i,j}) \}$$

$$\hat{A} = \frac{\partial \hat{E}}{\partial Q} = \hat{A}(Q_i, Q_{i+1})$$

The primitive-variable extrapolation of MUSCL approach is employed for higher order spatial accuracy. An implicit AF-ADI(Approximate

Factorization Alternating Direction Implicit) method<sup>9</sup> is used for time integration.

### 3. Grid System

The advantage of the embedded grid method lies in free choice of grid type<sup>10,11</sup>. In order to obtain accurate results, each grid must have sufficient resolution and satisfy orthogonality and smoothness. The base flow is divided into four zones - two for the rotor blades and two to convect the rotor-wake as shown in Fig.1.

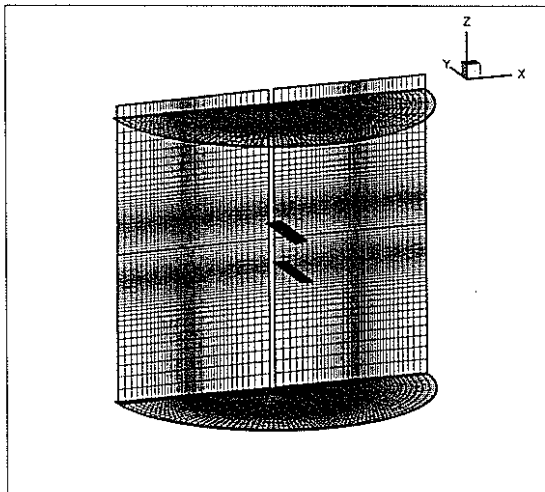


Fig.1 Side View of the Embedded Grid System

The larger H-type cylindrical grids around the each blade that cover the entire flow field are called as background grid<sup>12</sup>. Each of the background grid rotate in opposite direction on the sliding boundary, through which the flow information is exchanged. Fig 2 shows the fringe cells around the upper blade.

A moving patched grid method is also introduced to handle a sliding boundary. Since the proximity of the blade is of our primary interest, the background grids are clustered at the regions.

About  $8 \cdot 10^5$  grid points are used to construct the entire flow fields.

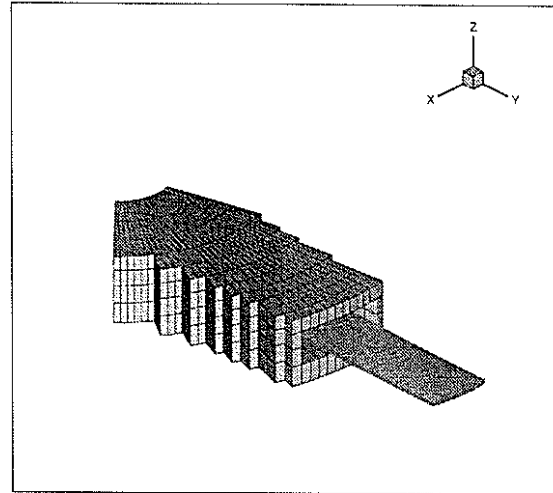


Fig.2 Fringe Points around the Rotor Blade

As mentioned above, the hovering flow field of a coaxial rotor system is inherently unsteady, the general blade motions must be described in the inertial coordinate. In this case, the motion of the grid points fixed at the blades are as follows<sup>13</sup>;

$$\begin{aligned} x_{\tau} &= -\Omega y - \mu M_{tip} \cos(\alpha_{TPP}) \\ y_{\tau} &= \Omega x \\ z_{\tau} &= 0 \end{aligned}$$

In addition, the every grid position and its metrics are updated in the following manner;

$$\begin{aligned} x^{n+1} &= x^n \cos(\Omega \Delta t) - y^n \sin(\Omega \Delta t) \\ y^{n+1} &= x^n \sin(\Omega \Delta t) + y^n \cos(\Omega \Delta t) \\ z^{n+1} &= z^n \end{aligned}$$

### 4. Boundary Condition

Since the blades are in motion in the present problem, the time metric should be included when imposing boundary conditions. Slip boundary condition is applied at the blade surfaces and the pressure is obtained from normal momentum

equation. There are two types of far boundary conditions available at the present. The one suggested by Srinivasan<sup>13</sup> is based on the three dimensional point-sink theory and mass conservation law. The method is known to avoid the "Closed Box" problem and shows a good convergency. However, it was originally developed for a single rotor and there is some doubt of its basic assumption. So, it can not be directly applied to the coaxial rotor calculation. The other is the characteristic far boundary condition based on the Riemann invariants. Although its convergency is not so good as the one, it produces a stable and reliable solutions<sup>14</sup>. Therefore, the latter method is adopted in the present work.

No flux condition is applied at the inboard boundary. It should be noted that this condition allows the cross flow along the span. In the wake capturing method, there exists a periodicity for a hovering rotor flow field. By introducing the periodic boundary, the entire computational domain can be reduced by  $1/2n$  ( $n$ : number of blade of each rotor)<sup>15</sup>. This is also true for the coaxial rotor flow field. The periodic boundary condition is used at the front and back wall boundaries.

The exchange of flow information between the half cylinders covering the blades is performed via sliding boundary. The accurate interpolation between the two zones is the most crucial factor in the present work. Fig. 3 is the top view of the sliding boundary and shows the schematic of the interpolation process.

As the calculation starts, each of the half cylinder rotates in the opposite direction. So, the sliding boundary is divided into the overlap region and

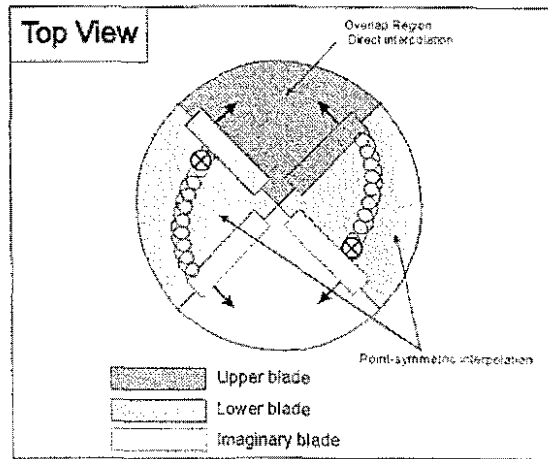


Fig. 3 The Schematic of Interpolation Process at the Sliding Boundary

non-overlap region. At the overlap region, the flow variables are directly interpolated but for the non-overlap region, the periodic nature of the flow field should be used again. If we assume the imaginary blades plotted in dashed line and the tip vortex generated from the upper blade goes out of the computational domain at point A, the same vortex must enters the lower half cylinder at point B. That is, the non-overlap region on the sliding boundary has the point-symmetric nature with respect to the center of rotation. Hence, for the non-overlap region, the point-symmetric interpolation should be accomplished. The detailed procedures are as follows; (1) the interpolation is performed on the entire sliding boundary; (2) determine the index that divides the overlap and non-overlap region; (3) the data-giving area is transformed in the point-symmetric way; (4) the interpolation is performed for the data-receiving area at the non-overlap region. In the present work, all interpolation is accomplished based on the angle that each cell occupies.

## 5. Vorticity Confinement Method

The vorticity confinement method (VCM, hereafter) involves computing a velocity correction to the solution from a conventional Euler/Navier-Stokes solver at each time step, which limits the spreading of a vortical regions due to numerical diffusion by convecting the vorticity back toward the centroid of the region<sup>16</sup>. The method is explained briefly here by considering the incompressible Navier-Stokes equations. With a confinement term, a set of modified Navier-Stokes equations are described as follows :

$$\nabla \cdot \mathbf{Q} = 0$$

$$\frac{\partial \mathbf{Q}}{\partial t} + (\mathbf{Q} \cdot \nabla) \mathbf{Q} = -\nabla \left( \frac{p}{\rho} \right) + \nu \nabla^2 \mathbf{Q} + \varepsilon \mathbf{K}$$

where  $\mathbf{Q}$  is the velocity,  $p$  pressure,  $\rho$  density. For the additional term,  $\varepsilon$  is a numerical coefficient which controls the size of the convecting vortical regions. The confinement term takes a simple form;

$$\mathbf{K} = -\hat{n} \times \omega$$

$$\hat{n} = \frac{\nabla \eta}{|\nabla \eta|}$$

where

$\omega = \nabla \times \mathbf{Q}$  is vorticity and  $\eta$  is a scalar field that has a local minimum on the centroid of the vortical region.

The main objective is to convect  $\omega$  back toward the centroid as it diffuses outward. In the confinement term,  $\hat{n}$  is a unit vector pointing away from the centroid of the vortical region. The coefficient  $\varepsilon$  is made to depend on the grid size so that the velocity correction becomes small in the region where the grid is fine enough<sup>17</sup>. One of the drawback of VCM is that there is no

general rule in the specification of  $\varepsilon$  and hence experience of the user is essential.

## 6. Results and Discussion

### Application of VCM

As noted in the previous section, VCM requires some experience in the specification of  $\varepsilon$ . In the case reported here,  $\varepsilon$  is determined from the cell volume ratio with the reference cell at the tip region. The value of  $\varepsilon$  at the reference cell depends on the grid density and varies from 0.4 to 0.65 in the present case. An hovering coaxial rotor calculation is performed in order to find out the effect of VCM. Tip mach number is 0.37 and the pitch angle is 7 degree for both rotors.

Thrust histories of the lower rotors with a variation of  $\varepsilon$  are depicted in Fig.4. Three cases ( $\varepsilon=0, 0.50$  and  $0.65$ ) are compared with one another. It is shown that overall trends are almost the same for all cases but in the case of  $\varepsilon=0.65$ , thrust is slightly underpredicted.

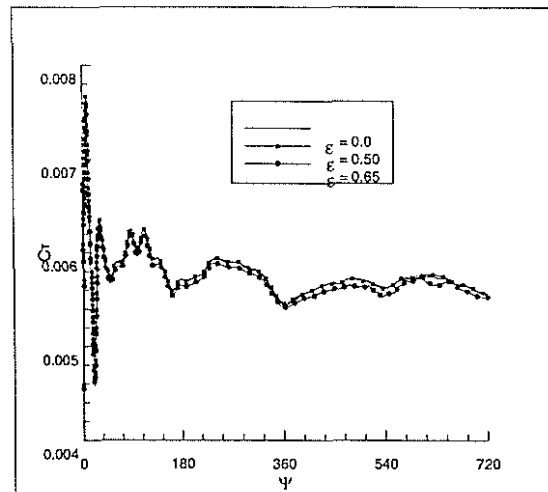


Fig. 4 Thrust History of the Lower Blade with a Variation of  $\varepsilon$ .

It should be noted that in the case of  $\varepsilon=0.65$ , the

thrust begins to oscillate at around  $\Psi=540$  where the tip vortices start to develop. Since velocity correction is added only in the presence of vorticity, it indicates that the numerical instability occurs due to the added velocity correction. If  $\epsilon$  has a value greater than 0.8, the solution diverges. Fig. 5 shows the density contours at  $\Psi=900$  deg. with a variation of  $\epsilon$ . It is clearly shown that the vortex core collapses with the increase of  $\epsilon$ .

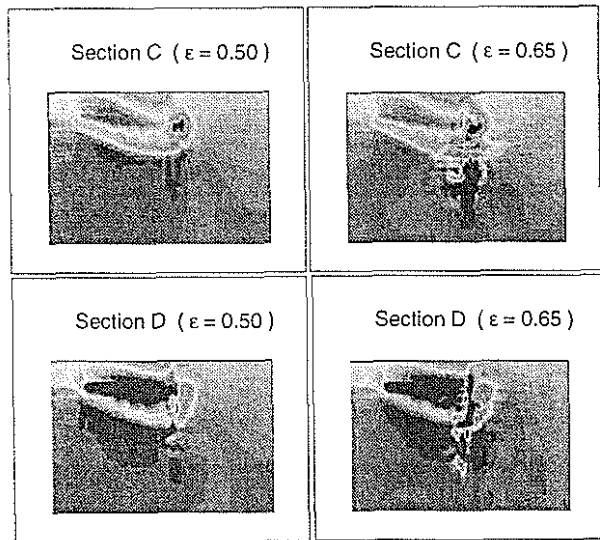


Fig.5 Density Contours at Two Different Sections with a Variation of  $\epsilon$ .

There seems to be two reasons for the instability of the solution;

- 1) It is very hard to specify proper values to  $\epsilon$  in the entire region. Because it is not possible to know the numerical diffusion rate all over the computational domain. Hence, if  $\epsilon$  exceeds the numerical diffusion rate at some points, the velocity correction becomes excessively large, resulting in a numerical instability;
- 2) Since in the 3-D calculation, the axis of the vorticity axis has an arbitrary direction, the outward normal vector  $\hat{n}$  may be miscalculated in the region where the

vorticity gradients varies abruptly.

Therefore, it is concluded that one should be careful when using vorticity confinement method because it may cause a numerical instability in case of wrong specification of  $\epsilon$ . So, in the following calculations, vorticity confinement method are not employed.

### Results of Coaxial Rotor Flowfield

As mentioned earlier, the coaxial rotor flow field is inherently unsteady unlike the single rotor. Therefore, one must use the unsteady code even for a hovering calculation and continue calculation until the solutions show a full periodicity. By introducing the sliding boundary, the computational domain is reduced by  $1/2n$  ( $n$ : the number of blade) but the accuracy of the solution depends on the interpolation at the sliding boundary. The volume ratio of the minor grid around the blade and the background grid plays an important role in the interpolation accuracy and the numerical stability. In a cylindrical grid system, the inboard grid is very dense and the grid becomes exponentially coarse along the radial direction. In this reason, there is much difficulty in controlling the cell volume ratio between the blade and the background<sup>18</sup>. It is well known that the trilinear interpolation does not satisfy the conservation law in itself. So the whole grid system is constructed so that the cell volume ratio does not exceed 5 to reduce the interpolation error.

Noticing that the previous researches concentrate the overall performance analysis, the present study tries to find out the unsteady nature of the coaxial flow field. The computation is

performed under the same condition as Nagashima's experiment<sup>3</sup>. The blade has the rectangular planform with aspect ratio of 6 and the NACA 0012 airfoil. The rotor tip velocity is Mach 0.37 and the pitch angles of the upper and lower rotor are 9° and 10°, respectively. The solidity is 0.1 and the rotor spacing, H/D is 0.2.

Fig.6 shows the thrust coefficient histories of the upper and lower rotors.

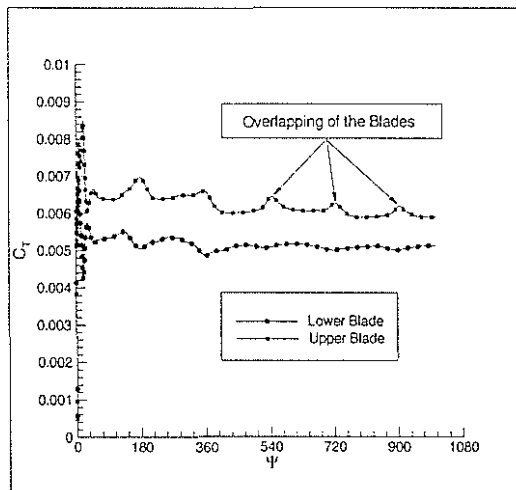


Fig. 6 Thrust Histories of the Upper and Lower Rotors

$\psi$  in the x-axis does not mean the azimuth angle but the angle displacement between the blades. So, it is twice the azimuth angle of the each blade. It is shown that the thrust coefficients oscillate until  $\psi$  reaches 90° due to the impulsive start. It is observed that at  $\psi = 180^\circ$ , the thrust of the upper rotor instantaneously increases while that of the lower rotor slightly decreases.

This is due to the increase of the effective pitch angle that happens when the two rotors overlap as shown in Fig.7.

The thrust coefficients are almost constant between the overlap of the rotors and the thrust increase of the upper rotor at the overlap location is about 8% of the mean thrust.

The calculated thrust coefficients are compared in Table 1 with the experiment and semi-empirical formula from "Helicopter" published in Russia<sup>19</sup>.

$C_T \cdot 10^2$	Upper Rotor	Lower Rotor	$(C_T)_l / (C_T)_u$
Present	0.6347	0.5229	0.824
Experiment (Ref. 3)	0.6217	0.3596	0.583
"Helicopter" (Ref. 19)	0.6731 ~ 0.8413	0.5793 ~ 0.7236	0.860

Table1 Comparison of Calculated Thrust and Load Sharing with Experiment and Semi-Empirical Formula

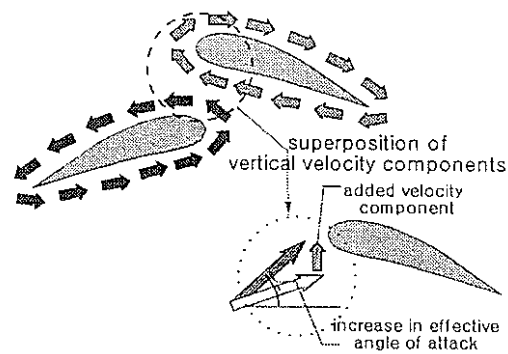


Fig. 7 Increase of the Effective Pitch Angle of the Upper Rotor

As shown in Table 1, the thrust of the upper rotor agrees well with the experiment, whereas the thrust of the lower rotor is over-predicted. This means that the downwash velocities from the upper rotor is under-estimated. It seems that as the tip vortex of the upper rotor passes through the computational domain, it diffuses out due to the numerical dissipation, thereby under-predicting the induced velocities.

It should be noted that the load sharing shows a good agreement with the semi-empirical results from "Helicopter". "Helicopter" is widely used for preliminary performance estimation. Considering that the experimental result shows a

large difference with that of "Helicopter"<sup>12</sup>, it is concluded that a more general and detailed experiment is required for the code validation.

The density contours are depicted at four circumferential locations when the two rotors overlap. Fig. 8 shows the cross sections of the wake grid where vortex was sampled.

The density contours for the lower rotor is shown in Fig. 9. At the section A, a tip vortex begins to form as it convects downward. By the time the tip vortex reaches the section B, the strength of the vortex core starts to weaken due to the numerical dissipation. The tip vortex at the section B re-enters the section C from the periodic boundary condition.

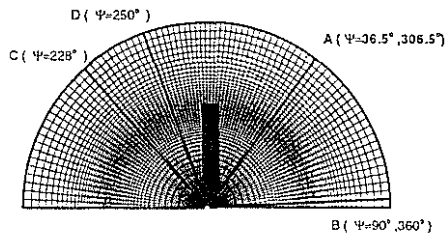


Fig.8 Cross Sections of Wake Grid Where Vortex was Sampled

As it contracts inward and descends downward, it reaches the section A. At the section A, two vortices can be observed. The lower one is generated from the preceding blade. The vortex diffuses out and lose its identity by the section D. It should be noted that the vortex sheet whose strength is weaker than vortex maintains its basic structure due to the dense grid at the inboard

area. The flow field of the lower rotor has almost the same trend as the upper one.

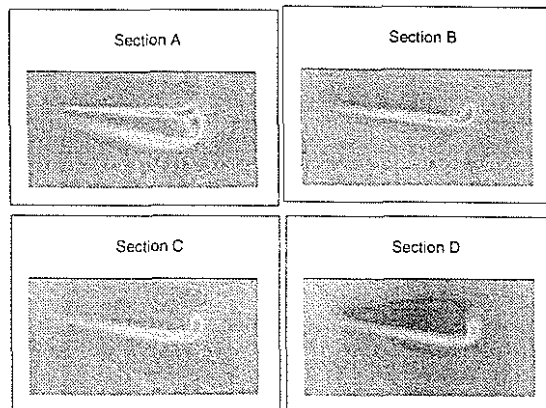


Fig. 9 The Density Contours for the Lower Rotor at Four Different Locations

It is observed that the strength of the tip vortex is weakened as it passes through the hole region. This stems from the successive interpolation and the accumulation of interpolation error.

The wake contraction and descent ratios are compared with the experimental data and Landgrebe's wake model in Fig. 10 and 11.

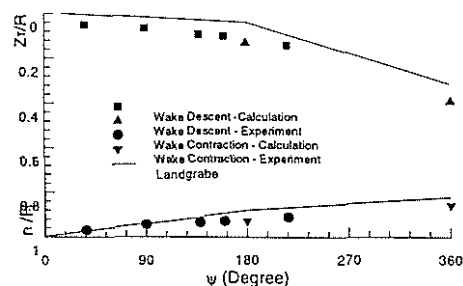


Fig. 10 Wake Contraction and Descent Ratio of the Upper Rotor

As shown in the figure, the calculated results show a similar trend as the experimental data but the wake descent ratio of the upper rotor is under-predicted. It is thought that the induced velocities

are under-predicted due to the rapid diffusion of the tip vortex of the upper rotor. For the lower rotor, the contraction ratio shows a difference with experimental data. It seems that the outflow boundary condition at the bottom of the lower wake grid has an effect on this problem and this subject will be addressed in another paper.

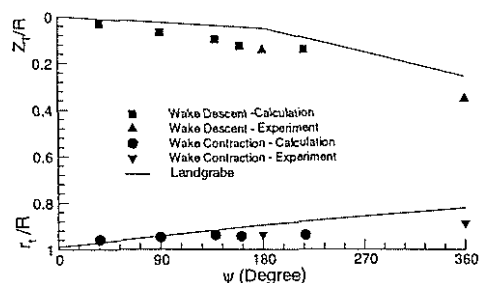


Fig. 11 Wake Contraction and Descent Ratio of the Lower Rotor

## 6. Concluding Remark

The present study investigates the unsteady flow fields around the coaxial rotor by using the up-to-date numerical analysis technique. The primary objectives are to find out the unsteady aerodynamic characteristics of the coaxial rotor flow field and to provide a basic numerical tools for further researches. To achieve this goal, the numerical analysis code was developed to handle the moving rotor configuration. By applying the present code to the three-dimensional coaxial rotor flow field analysis, the following conclusions are reached:

(1) Therefore, it is concluded that one should be careful when using vorticity confinement method

because it may cause a numerical instability in case of wrong specification of  $\epsilon$ ; (2) The rotor analysis code for the unsteady coaxial flow field has been developed and the calculated results shows good agreements with the experimental data; (3) The tip vortex and vortex sheet diffuse out within one revolution but wake contraction and descent ratios agree well with the experimental data. Further researches are required to minimize the numerical diffusion such as the use of less diffusive numerical scheme and denser grid system; (4) The sliding boundary is introduced to efficiently construct the computational domain and the interpolation strategy is suggested.

## Reference

1. Colin P. Coleman, "A Survey of Theoretical and Experimental Coaxial Rotor Aerodynamic Research", 19<sup>th</sup> European Rotorcraft Forum, 1993, pp. D.11.1-11.28
2. Alfred Gessow and Gary C. Myers, Jr., *Aerodynamics of the Helicopter*, Frederic Ungar Publishing Co. 1967
3. T. Nagashima and K. Nakanishi, "Optimum Performance and Load Sharing of Coaxial Rotor in Hover", *Journal of Japan Society for Aeronautics and Space Sciences*, Vol. 26, No. 293, June 1978, pp. 325-333
4. S. Saito and A. Azuma, "A Numerical Approach to Coaxial Rotor Aerodynamics", Proceedings of the 7<sup>th</sup> European Rotorcraft and Powered Lift Forum, Vol. 24, No. 42, 1981
5. Anton J. Landgrebe, "The Wake Geometry of a Hovering Helicopter Rotor and its

- Influence on Rotor Performance”, Proceedings of the 28<sup>th</sup> Annual Forum of American Helicopter Society, 1972
6. Brian E. Wake,” Solution Procedure for the Navier-Stokes Equations Applied to Rotors”, Ph. D Dissertation, Georgia Institute of Technology, 1987
  7. R. K. Agarwal and J. E. Deese, “Euler Calculations for Flowfield of a Helicopter in Hover”, *Journal of Aircraft*, Vol.24, No. 4, April 1987
  8. P. L. Roe, “Approximate Riemann Solvers, Parameter Vectors and Difference Schemes”, *Journal of Computational Physics*, Vol.43, No.3 , 1981, pp.357-372
  9. J. L. Steger and R. F. Warming, “ Flux Vector Splitting of the Inviscid Gasdynamic Equations with Application to Finite Difference Methods”, *Journal of Computational Physics*, Vol.40, pp.263-293
  10. Dougherty, F.C. ,”Development of a Chimera Grid Scheme with Applications to Steady Problems”, Ph. D Dissertation, Stanford University, 1985
  11. Joseph L. Steger and John A. Benek, “On the Use of Composite Grid Schemes in Computational Aerodynamics”, *Computer Method in Applied Mechanics and Engineering*, Vol.64, 1987, pp. 310-320
  12. Earl-Peter N. Duque and G. R. Srinivasan,” Numerical Simulation of a Hovering Rotor Using Embedded Grids”, AHS 48<sup>th</sup> Annual Forum and Technology Display, Washington D.C., 1992
  13. G. R. Srinivasan and J. D. Baeder, “TURNS: A Free-Wake Euler/Navier-Stokes Numerical Method for Helicopter Rotors”, *AIAA Journal*, Vol. 31, No.5, May 1993, pp. 959-962
  14. E. Kramer, J. Hertel and S. Wagner,” Euler Procedure for Calculating of the Steady Rotor Flow with Emphasis on Wake Evolution”, AIAA-90-3007-CP
  15. K. Pahkle and J. Raddatz, “ 3D Euler Methods for Multi-Bladed Rotors in Hover and Forward Flight”, 19<sup>th</sup> European Rotorcraft Forum, Paper No. C20
  16. John Steinhoff and G.K. Raviprakash,” Navier-Stokes Computation of Blade-Vortex Interaction Using Vorticity Confinement”, AIAA 95-0161-CP,33<sup>rd</sup> Aerospace Sciences Meeting and Exhibit, January 9-12, 1995, Reno,NV
  17. J.Steinhoff and D.Underhill,”Modification of the Euler Equations for “Vorticity Confinement” - Application to the Computation of Interacting Vortex Rings”, *Physics of Fluids*, Vol.6, 2738(1994)
  18. Takeshi Sakata and Anthony Jameson,”Multi-Body Flow Field Calculations with Overlapping Mesh Method”, AIAA-89-2179-CP
  19. L.S.Vil'dgrude,”Helicopters-Calculation and Design”, NASA TTF-519